Int. J. Electrochem. Sci., 10 **(2015)** 303 - 316

International Journal of
ELECTROCHEMICAL
SCIENCE
www.electrochemsci.org

Simultaneous Determination of Hydroxylamine, Phenol and Sulfite in Water and Waste Water Samples Using A Voltammetric Nanosensor

Vinod Kumar Gupta[1, 2,*], *Hassan Karimi-Maleh*[*3,4] ,*Roya Sadegh*[3]

[1]Department of Chemistry, Indian Institute of Technology Roorkee, Roorkee 247667, India
[2]Department of Applied Chemistry, University of Johannesburg, Johannesburg, South Africa
[3]Department of Chemistry, Majlesi Branch, Islamic Azad University, Isfahan, Iran
[4] Department of Chemistry, Graduate University of Advanced Technology, Kerman, Iran
[*]E-mail: vinodfcy@gmail.com; h.karimi.maleh@gmail.com

Received: 22 August 2014 / *Accepted:* 11 October 2014 / *Published:* 17 November 2014

This paper describes the development a novel 8,9-dihydroxy-7-methyl-12H-benzothiazolo[2,3-b]quinazolin-12-one -ZnO/CNTs modified carbon paste electrode (DMBQ/ ZnO/CNTs/CPE)for the electrocatalytic determination of hydroxylamine (HX) in the presence of phenol (PL) and sulfite (ST) in water and waste water samples. We describe synthesis and characterization of ZnO/CNTs nanocomposite with different methods such as Scanning electron microscopy (SEM); Energy-dispersive X-ray spectroscopy (EDS) and X-ray diffraction (XRD). Result shows for the mixture containing HX, PL and ST, the peaks potential well separated from each other. Their square wave voltammetrics (SWV) peaks current increased linearly with their concentration at the ranges of 0.09–350, 0.5–500 and 0.7–400 μM, respectively with the detection limits of 0.04, 0.1 and 0.3 μM, respectively. The modified electrode was successfully used for the determination of the analytes in real samples with satisfactory result.

Keywords: Hydrazine; Phenol; Water and waste water analysis; Voltammetric Sensor, ZnO/CNTs nanocomposite

1. INTRODUCTION

Hydroxylamine is a reducing agent that is useful in biochemical cross linking applications, including the deacetylation of *N*-succinimidyl *S*-acetylthioacetate (SATA) and chemical cleavage of Ethylene glycol bis [succinimidylsuccinate] (EGS) and Sulfo-EGS [1]. Hydroxylamine's production and use as a reducing agent and intermediate in the production of caprolactam may result in its release

to the environment through various waste streams. On the other hand, HX may explode on heating and the nature of the explosive hazard is not well understood [2]. Also, HX is an irritant to the respiratory tract, skin, eyes, and other mucous membranes. It may be absorbed through the skin, is harmful if swallowed, and is a possible mutagen. Therefore, the quantitative determination of HX is very significant in environmental samples such as water and waste water.

Phenol is a high toxicity compound in environmental samples that is subject to regulation as water pollutants [3]. Phenol is highly irritating to the skin, eyes, and mucous membranes in humans after acute (short-term) inhalation or dermal exposures. On the other hand, PL is considered to be quite toxic to humans via oral exposure. Anorexia, progressive weight loss, diarrhea, vertigo, salivation, a dark coloration of the urine, and blood and liver effects have been reported in chronically (long-term) exposed humans. Animal studies have reported reduced fetal body weights, growth retardation, and abnormal development in the offspring of animals exposed to phenol by the oral route [4].

Sulfites are commonly used in the food industries as preservatives and antioxidants, and in the brewing industry as an antibacterial agent. Sulfites occur naturally in all wines to some extent. Sulfites are commonly introduced to arrest fermentation at a desired time, and may also be added to wine as preservatives to prevent spoilage and oxidation at several stages of the winemaking. Without sulfites, grape juice would quickly turn to vinegar. In large quantities, sulfite and its oxidation products are pollutants [5]. High sulfite content in the blood and urine of babies can be caused by molybdenum cofactor deficiency disease which leads to neurological damage and early death unless treated. Treatment, requiring daily injections, became available in 2009 [6].

According to the above points, it is very vital for design and construction of a rapid and inexpensive sensor for analyzing of HX, PL and ST in real samples. Health survey of drinking water and wastewater can be useful for human health. Some publications are available regarding electrochemical determination of just HX in real samples using chemically modified electrodes [7-9]. In all of the reported papers, PL and ST acts as an interfering compound, hence needing separation before analysis, because it affects the selectivity. As yet, based on our knowledge, no paper has been reported on the simultaneous determination of HX pulse PL and ST using electrochemical methods. Therefore, in continuation of our studies concerning the preparation of chemically modified electrodes for electroactive compounds analysis [10–20], in the present work, we describe preparation of a new DMBQ/ ZnO/CNTs/CPE and investigate its performance for the electrocatalytic determination of HX in aqueous solutions. We also evaluate the analytical performance of the modified electrode for simultaneous determination of HX, PL and ST.

2. EXPERIMENTAL

2.1. Chemicals

All chemicals used were of analytical reagent grade purchased from Merck (Darmstadt, Germany) unless otherwise stated. Double distilled water was used all throughout the experiments.

1.0×10^{-2} mol L^{-1} HX solution was prepared daily by dissolving 0.0640 g HX in water and the solution was diluted to 100 mL with water in a 100–mL volumetric flask. The solution was kept in a refrigerator at 4 ^{o}C in the dark. Further dilution was made with water.

1.0×10^{-2} mol L^{-1} PL solution was prepared daily by dissolving 0.094 g PL in a buffer solution, pH = 8.0, in a 100–mL volumetric flask, and under ultrasonication for several minutes. Further dilution was made with water.

1.0×10^{-2} mol L^{-1} ST solution was prepared daily by dissolving 0.013 g ST in a buffer solution, pH = 8.0, in a 100–mL volumetric flask, and under ultrasonication for several minutes. Further dilution was made with water.

Phosphate buffer solutions (sodium dihydrogen phosphate and disodium monohydrogen phosphate plus sodium hydroxide, 0.1 mol L^{-1}), PBS, with different pH values were used.

High viscosity paraffin (d = 0.88 kg L^{-1}) from Merck was used as the pasting liquid for the preparation of carbon paste electrode. Spectrally pure graphite powder (particle size<50 μm) from Merck and multiwall carbon nanotubes (>90% MWNT basis, d × l = (90 – 60 nm) × (5 – 9 μm)) from Fluka were used as the substrate for the preparation of the carbon paste electrode as a working electrode.

2.2. Apparatus

Cyclic voltammetry (CV), impedance spectroscopy, and square wave voltammetry (SWV) were performed in an analytical system, Autolab with PGSTAT 302N (Eco Chemie, the Netherlands). The system was run on a PC using GPES and FRA 4.9 software. For impedance measurements, a frequency range of 100 kHz to 1.0 Hz was employed. The AC voltage amplitude used was 5 mV, and the equilibrium time was 15 min. A conventional three-electrode cell assembly consisting of a platinum wire as an auxiliary electrode and an Ag/AgCl (KCl_{sat}) electrode as a reference electrode were used. The working electrode was either an unmodified carbon paste electrode (CPE) or a DMBQ/ ZnO/CNTs/CPE.

2.3. Synthesis of ZnO/CNTs

The commercial multiwalled carbon nanotubes with tube diameters of about 10–20 nm were used. The preparation of ZnO/CNTs catalysts includes three steps. First, the chemical pretreatment of carbon nanotubes is required. A definite amount of carbon nanotubes was introduced into 40 cm^3 of nitric acid and sulfuric acid (3:1 in volume) solution; then, 10 cm^3 of ethanol was dropped into the solution slowly, and the solution was agitated in a shaker at 65 °C and 200 rpm for 24 h. In the second step, certain amounts of purified CNTs (3 g) were dispersed into distilled water solution of NaOH (0.5 M; 100 mL) by ultrasonication for 20 min. The third step is the supporting of zinc oxide on carbon nanotubes by a direct deposition process. $Zn(NO_3)_2.2H_2O$ of 3.7 g was dissolved in 100-mL distilled water. Under constant magnetic stirring, the solution of $Zn(NO_3)_2.2H_2O$ was added dropwise to the solution of CNTs at 50 °C through a dropping funnel. The rate of addition of the salt solution was kept

approximately at 20 mL h^{-1}. After completion of the precipitation procedure, the mixture was stirred at room temperature for 18 h, washed and filtered continually in distilled water (pH 7.5), and dried at 120 °C. The solid samples were then calcined at 250 °C for 2 h.

2.4. Preparation of the modified electrode

For obtained the best condition in preparation of modified electrode, we optimized ratio ZnO/CNTs and DMB in DMBQ/ ZnO/CNTs/CPE. The result shows that the maximum intensity is used in 15.0% w/w ZnO/CNTs and 2.5% w/w DMBQ. Therefore, we selected these conditions of 15.0% w/w ZnO/CNTs and 2.5% w/w DMBQ for preparation of modified electrode. To prepare the modified electrode 25.0 mg of DMBQ was hand mixed with 825.0 mg of graphite powder and 150.0 mg of ZnO/CNTs in a mortar and pestle. Using a syringe, 12 drops of paraffin were added to the mixture and mixed well for 45 min until a uniformly wetted paste was obtained. The paste was then packed into a glass tube. Pushing a copper wire down the glass tube into the back of the mixture made electrical contact. When necessary, a new surface was obtained by pushing an excess of the paste out of the tube and polishing it on a weighing paper. The unmodified carbon paste electrode (CPE) was prepared in the same way without ZnO/CNTs and DMBQ to the mixture to be used for the comparison purposes.

2.5. Preparation of real samples

Water samples were stored in a refrigerator immediately after collection. Ten milliliters of the sample was centrifuged for 10 min at 2000 rpm. The supernatant was filtered using a 0.45 μm filter and then diluted 2–times with the PBS pH = 8.0. The solution was transferred into the voltammetric cell to be analyzed without any further pretreatment. The standard addition method was used for the determination of HX, PL and ST.

Without any pre-treatment of the sample, an accurate volume of the boiler water depending on the amount of above compounds in the sample (commonly 0.2–1.0 mL) directly was subjected for voltammetric measurement of above compounds as recommended procedure.

3. RESULTS AND DISCUSSION

3.1 ZnO/CNTs characterization

ZnO/CNT nano-powders were analyzed by XRD analyses. The XRD pattern of ZnO/CNT nano-powders, in the 2θ range of 10–80°, is shown in Fig. 1A. The prominent peaks were used to calculate the grain size via the Scherrer equation, expressed as follows:

$$D=K\lambda/(\beta \cos\theta) \quad (1)$$

Where λ is the wavelength (λ = 1.542 Å) (CuK_α), β is the full width at half maximum (FWHM) of the line, and θ is the diffraction angle. The grain size of the ZnO nanoparticle was 22.0 nm, and the

peaks were observed at the (100), (002), (101), (102), (110), (103), (200), (112), (201), (004) and (202) planes (for FCC structure). These peaks correspond to ZnO. Also, it clearly proves the presence of CNTs with a diffraction peak at about 26°. Figure 1B presents a typical TEM image of ZnO/CNT nanocomposite. Result shows the core of particles supported on carbon nanotubes. Since the corresponding XRD pattern is only CNTs and ZnO, it was believed that the core and nanotubes of particles should be ZnO and carbon nanotubes, respectively.

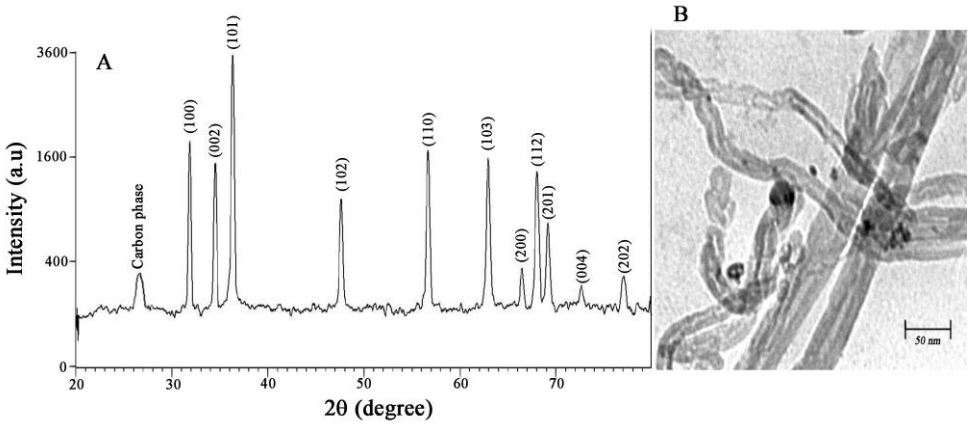

Figure 1. A) XRD patterns of as-synthesized ZnO/CNTs nanocomposite. B) TEM image of ZnO/CNTs.

3.2. Catalytic Effect

Figure 2 depicts the cyclic voltammetric responses from the electrochemical oxidation of 300 μM HX solution at DMBQ/CPE (curve b), at DMBQ/ZnO/CNTs/CPE (curve c), at ZnO/CNTs/CPE (curve d), and at CPE (curve e). Also, the curve a and curve f (Fig. 2) show the CVs of DMBQ/ZnO/CNTs/CPE and ZnO/CNTs/CPE in the buffer solution (pH 8.0), respectively. As can be seen, the anodic peak potential for oxidation of HX at DMBQ/ ZnO/CNTs/CPE (curve c) and at DMBQ/CPE (curve b) was about 240 mV, while it was about 990 mV at ZnO/CNTs/CPE (curve d). At the unmodified CPE, the peak potential of HX was about 1050 mV (curve e). From these results, it was concluded that the best electrocatalytic effect for HX oxidation was observed at DMBQ/ ZnO/CNTs/CPE (curve c). For example, the results show that the peak potential of HX oxidation at DMBQ/ZnO/CNTs/CPE (curve c) shifted by about 750 mV and 810 mV toward negative values when compared to that at ZnO/CNTs/CPE (curve d) and at CPE (curve e), respectively. Likewise, when comparing the oxidation of HX at DMBQ/ZnO/CNTs/CPE (curve c) relative to that at DMBQ/CPE (curve b), a dramatic enhancement was observed in the anodic peak current at DMBQ/ ZnO/CNTs/CPE. In other words, the data clearly show that the combination of ZnO/CNTs and the DMBQ definitely improves the characteristics of HX oxidation. This behavior is typical of that expected for electrocatalysis at chemically modified electrodes [21-27].

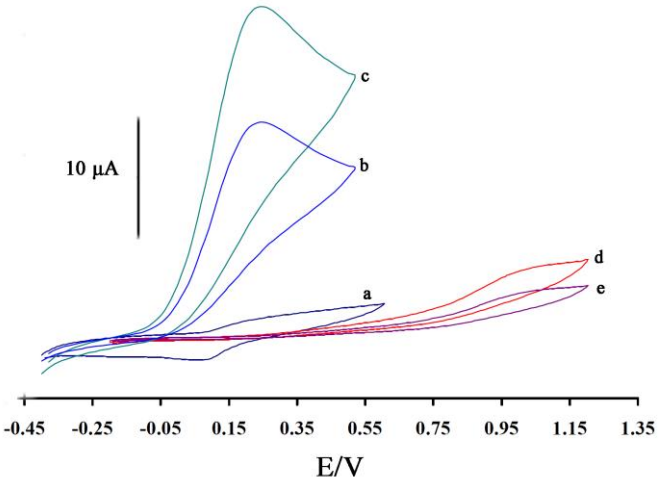

Figure 2. Cyclic voltammograms of (a) the buffer solution at DMBQ/ZnO/CNTs/CPE; (b) 300 µM HX at DMBQ/CPE; (c) 300 µM HX at DMBQ/ZnO/CNTs/CPE; (d) 300. µM HX at ZnO/CNTs/CPE; (e) 300 µM HX at CPE. Conditions: 0.1 mol L^{-1} PBS (pH 8.0), scan rate of 20 mV s^{-1}.

The influence of potential scan rate (ν) on catalytic current (I_p) of HX at DMBQ/ ZnO/CNTs/CPE was studied by cyclic voltammetry at various sweep rates (Fig. 3 inset A). Results show that the peak currents of HX grow with the increasing of scan rates and there are good linear relationships between the peak currents and the square root of the scan rate ($\nu^{1/2}$) (Fig.3). Also, they show that the action is mass transfer controlled at the sufficient over-potentials [28-30]. The recorded CVs showed a positive shift in E_p, which is confirming the kinetic limitation in the electrochemical reaction [30-35]. Interestingly, the current function plot (Fig. 3, inset B) gave the characteristic shape of acoupled chemical reaction (EC_{cat}) for the hydrazine, clearly confirming the electrocatalytic activity of the mediator.

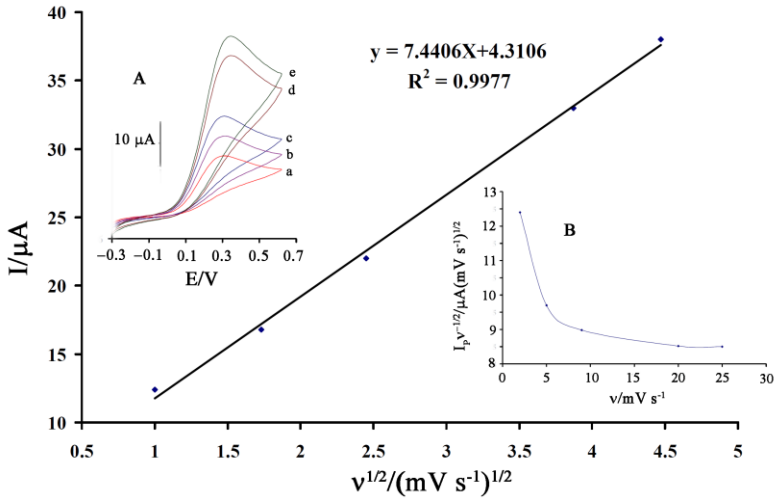

Figure 3. Plot of I_{pa} versus $\nu^{1/2}$ for the oxidation of 200.0 µM HX at various scan rates of (a) 1.0; (b)3.0; (c) 6.0; (d) 15.0; and (e) 20.0 mV s^{-1} in 0.1 mol L^{-1} phosphate buffer solution(pH 8.0) at DMBQ/ZnO/CNTs/CPE. Inset A) Cyclic voltammograms of 200.0 µM HX at various scan. Insert B) variation of the scan rate-normalized current ($I_p/\nu^{1/2}$) with scan rate.

To obtain information about the rate-determining step, the Tafel plot was drawn, as derived from points in the Tafel region of the cyclic voltammogram (Fig. 4). The slope of the Tafel plot was equal to 2.3RT/ n(1−α)F , which came up to 0.2393 and 0.2373 V decade^{-1} for scan rates 1 and 6 mV s^{-1}, respectively. Therefore, we obtained the mean value of α equal to 0.7. In addition, the value of α was calculated for the oxidation of HX at pH 8.0 for both of the DMBQ/ZnO/CNTs/CPE and CPE using the equation (1):

$$\alpha n_\alpha = 0.048/(E_P - E_{P/2}) \quad (1)$$

where $E_{P/2}$ is the potential corresponding to $I_{P/2}$. The values for αn_α were found to be 0.7 and 0.2 at the surface of both of DMBQ/ZnO/CNTs/CPE and the CPE, respectively. The values show that the over–potential of HX oxidation is reduced at the surface of DMBQ/ZnO/CNTs/CPE, and also that the rate of electron transfer process is greatly enhanced. This phenomenon is, thus, confirmed by the larger I_{pa} values recorded during the cyclic voltammetry at DMBQ/ZnO/CNTs/CPE.

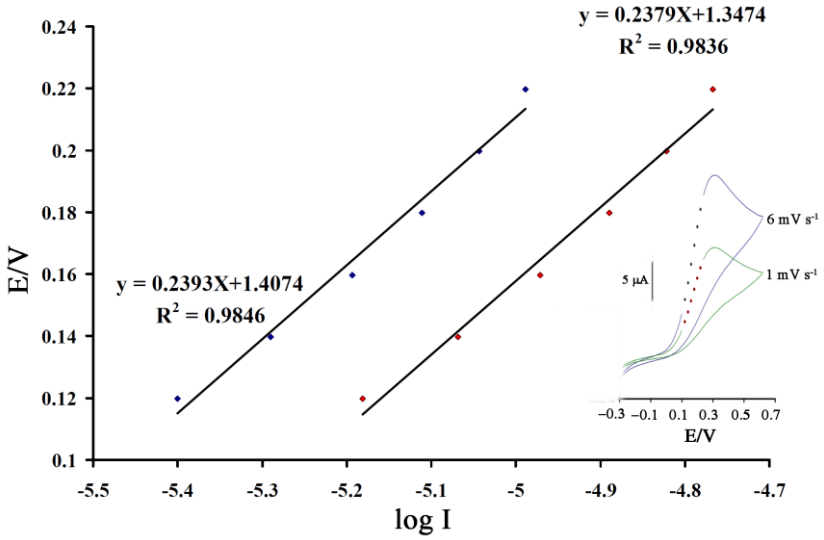

Figure 4. Tafel plot for DMBQ/ZnO/CNTs/CPE in 0.1 mol L^{-1} PBS (pH 8.0) with scan rates of 1 and 6 mV s^{-1} in the presence of 200.0 μM HX.

In chronoamperometric studies, we determined the diffusion coefficient (D) of HX. The experimental plots of I vs. t$^{-1/2}$ were employed with the best fits for different concentrations of HX. Chronoamperometric measurements for different concentrations of HX at DMBQ/ZnO/CNTs/CPE were accomplished by setting the working electrode potential at 0.0 and 0.5 V as the first- and second-step potentials (Fig. 5A). The slopes of the resulting straight lines were then plotted vs. HX concentrations using the Cottrell equation to obtain the following equation [36]:

$$I = nFAD^{1/2}C_b\pi^{-1/2}t^{-1/2} \quad (2)$$

where D and C_b are the diffusion coefficient (cm^2 s^{-1}) and the bulk concentration (mol cm^{-3}), respectively. On other hand, A and F are the surface area of the working electrode 0.09 cm^2 and Faraday constant 96,485 C/mol. Under diffusion control, plot of i vs. t$^{-1/2}$ will be linear in different concentration of HX, and the mean value of D can be obtained from the slopes (Fig. 5B). The diffusion coefficient for HX was calculated as 7.13×10^{-5} cm^2 s^{-1}.

Chronoamperometry can also be employed to evaluate the catalytic rate constant, k_h for the reaction between HX and DMBQ/ZnO/CNTs/CPE according to the method of Galus [37]:

$$I_C/I_L=\gamma^{1/2}[\pi^{1/2}\mathrm{erf}(\gamma^{1/2}) + \exp(-\gamma)/\gamma^{1/2}] \quad (3)$$

where I_C is the catalytic current of HX at DMBQ/ZnO/CNTs/CPE, I_L is the limiting current in the absence of HX and $\gamma=k_hC_bt$ (C_b is the bulk concentration of HX) is the argument of the error function. In the cases where γ exceeds two the error function is almost equal to 1 and therefore, the above equation can be reduced to:

$$I_C/I_L= \gamma^{1/2}\ \pi^{1/2}=\pi^{1/2}\ (k_hC_bt)^{1/2} \quad (4)$$

where t is the time elapsed in seconds. The above equation can be used to calculate the rate constant of the catalytic process k_h. Based on the slope of I_C/I_L *vs.* $t^{1/2}$ plot, k_h can be obtained for a given HX concentration (Fig. 5C). From the values of the slopes, an average value of k_h was found to be $k_h=5.245 \times 10^3$ mol^{-1} L s^{-1}. The value of k_h explains as well as the sharp feature of the catalytic peak observed for catalytic oxidation of HX at the surface of DMBQ/ZnO/CNTs/CPE.

Double potential step chronocoloumetry, as well as other electrochemical methods, was also employed for the investigation of the electrode processes at DMBQ/ZnO/CNTs/CPE in the absence of the presence of HX. Forward and backward potential step chronocoloumetry on the modified electrode in a blank buffer solution showed very symmetrical chronocolougrams. These had about an equal charge consumed for both oxidation and reduction of $DMBQ_{Red}/DMBQ_{Ox}$ redox system in DMBQ/ZnO/CNTs/CPE. However, in the presence of HX, the charge value associated with forward chronocoloumetry was significantly greater than that observed for the backward chronocoloumetry (Fig. 5D). This behavior is typical of that expected for electrocatalysis at chemically modified electrode [38-43].

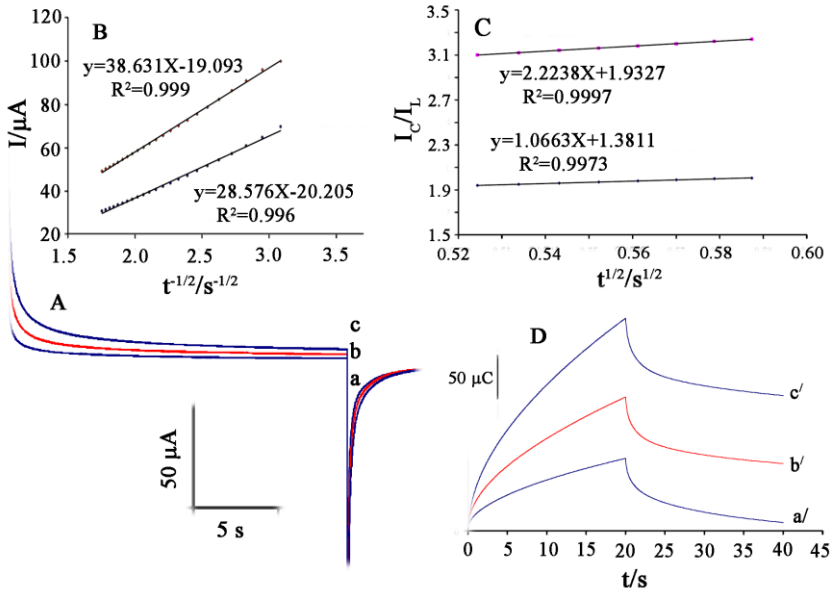

Figure 5. (A) Chronoamperograms obtained at DMBQ/ZnO/CNTs/CPE (a) in the absence, and in the presence of (b) 150.0 μM; (c) 200 μM HX at pH 8.0. (B) Cottrell's plot for the data from the chronoamperogram. (C) Dependence of I_c/I_L on the $t^{1/2}$ derived from the chronoamperogram data. (D) The charge–time curves ($a^{/}$) for curve (a); ($b^{/}$) for curve (b) and ($c^{/}$) for curve (c).

3.3. Electrochemical impedance spectroscopic study

Electrochemical impedance spectroscopy (EIS) is one of the most effective and reliable electrochemical methods to extract information about electrochemical characteristics of the electron-exchange systems, including double-layer capacitance, diffusion impedance, determination of the rate of charge transfer and charge transport processes, electrocatalytic systems and solution resistance [44-46].

So, EIS was also employed to investigate HX, PL and ST oxidation at DMBQ/ZnO/CNTs/CPE. The electrical equivalent circuits (from the modified electrode in the absence and presence of HX, PL or ST) compatible with the impedance spectra are shown in figure 6 inset. In this circuit, R_s, Q, and R_{ct} represent solution resistance, a constant phase element corresponding to the double-layer capacitance, and the charge transfer resistance associated with the oxidation of low-valence mediator species. W is a finite-length Warburg short-circuit term coupled to R_{ct}. Fig. 6 presents the Nyquist diagrams and bode plots of the imaginary impedance (Z_{im}) vs. the real impedance (Z_{re}) of the EIS obtained at the modified electrode recorded at 0.1 V dc-offset in the absence (a) and in the presence of 300 µM PL (b); in the presence of 300 µM ST and 300 µM HX (c) in 0.1 M PBS (pH 8.0), respectively. As can be seen in high frequencies; there is a depressed semicircle that may be related to the combination of charge transfer resistance of electroactive material at a surface of electrode and double-layer capacitance (see Fig. 6 inset).

.

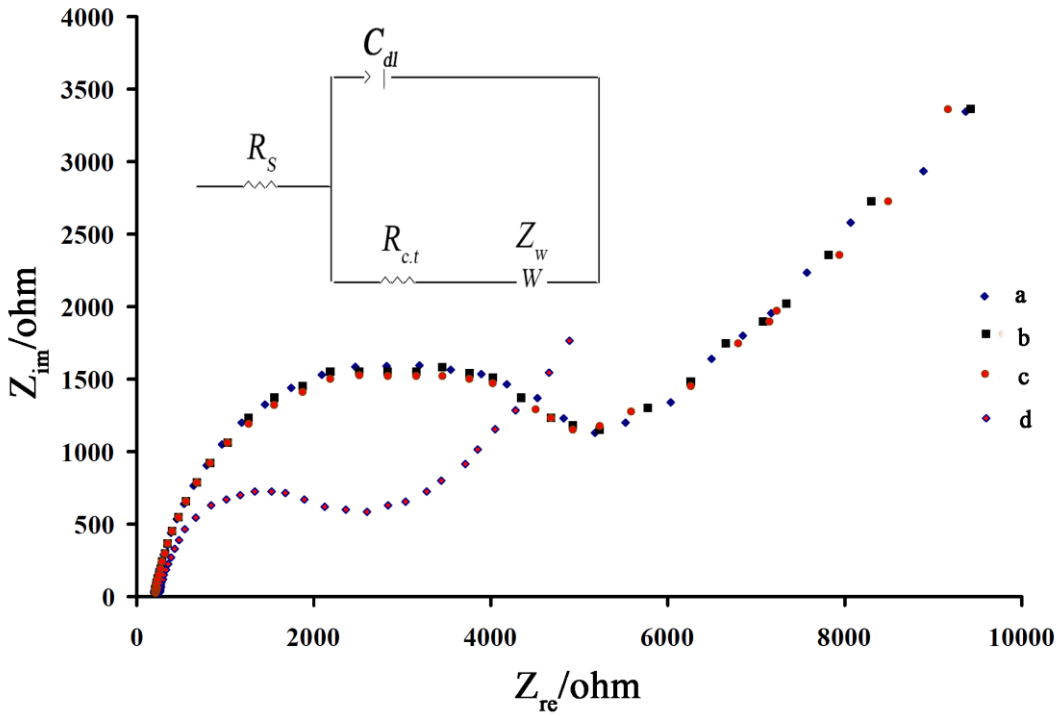

Figure 6. Nyquist diagrams of DMBQ/ZnO/CNTs/CPE (a) in the absence; (b) in the presence of 300 µM PL; (c) in the presence of 300 M ST and (d) in the presence of 300 M HX . Inset shows the related bode plots of (a), (b), and (c).

In following, a straight line with a slope of nearly 45◦ shows in Nyquist diagrams that related to mass transport process via diffusion of electroactive compound. In the presence of HX, the diameter of the semicircle decreases, confirming the electrocatalytic capability of the mentioned electrocatalyst for the oxidation of HX. This is due to the instant chemical reaction of HX with the high-valence ethynylferrocene species. It is evident from the EIS data that, in the presence of HX at a surface of the modified electrode, the resistance to electron transfer was at its minimum value. Therefore, there must be an interaction between HX and the mediator in the mediator potential oxidation. The catalytic reaction of HX oxidation that occurred via the participation of DMBQ species virtually caused an increase in the surface concentration of low valence species of the electrocatalyst. Thus, the charge-transfer resistance declined, depending on the concentration of HX in the solution.

On the other hand, PL and ST were not able to be electrocatalyzed on this modified electrode to provide the necessary conditions for the selective determination of HX in real samples. This behavior is consistent with the result of cyclic voltammetry and chronoamperometry

3.4 Calibration plot and detection limit

SWV has a much higher current sensitivity and better resolution than cyclic voltammetry, the SWV was used for the simultaneous determination of HX, PL and ST. In order to get the best sensitivity under the specific condition, an amplitude potential of 50 mV and frequency of 12 Hz were selected. The plot of peak current *vs.* the HX concentration consisted of two linear segments with slopes of 0.7548 and 0.1616 $\mu A/\mu M^{-1}$ at the concentration ranges of 0.09–9.9 μM and 9.0–350.0 μM, respectively. The decreasing of sensitivity (slope) of the second linear segment is likely due to kinetic limitation. On the other hand, the responses were linear with the PL concentration at the range from 0.5 to 500.0 μM and the current sensitivity was 0.0195 $\mu A/\mu M^{-1}$, while the dynamic range was linear with the ST concentration at the range from 0.7 to 400 μM and the current sensitivity was 0.0308 $\mu A/\mu M^{-1}$. The detection limits were determined as 0.04 μM for HX; 0.1 μM for PL and 0.3 μM for ST based on $Y_{LOD} = Y_B+3\sigma$.

3.5 Simultaneous determination of HX, PL and ST

One of the main objectives of this study was to develop a modified electrode with the capability of separating the electrochemical responses of HX, PL and ST in aqueous solution. Using DMBQ/ZnO/CNTs/CPE as the working electrode; the analytical experiments were carried out by varying the concentration of DMBQ/ZnO/CNTs/CPE in 0.1 M PBS (pH 8.0). The SW voltammetric results show three well-distinguished anodic peaks at potentials of 160, 530 and 840 mV, corresponding to the oxidation of HX, PL and ST, respectively, indicating that the simultaneous determination of HX, PL and ST is possible at the DMBQ/ZnO/CNTs/CPE (Fig. 7 inset). The sensitivities of the modified electrode towards HX in the absence (0.7548 $\mu A\mu M^{-1}$) and presence (0.7329 $\mu A\mu M^{-1}$) of PL and ST are virtually the same, which further indicate that the oxidation

processes of HX, PL and ST at the DMBQ/ZnO/CNTs/CPE are independent and therefore, simultaneous measurements of the three analytes are feasible without any interference (Fig. 7).

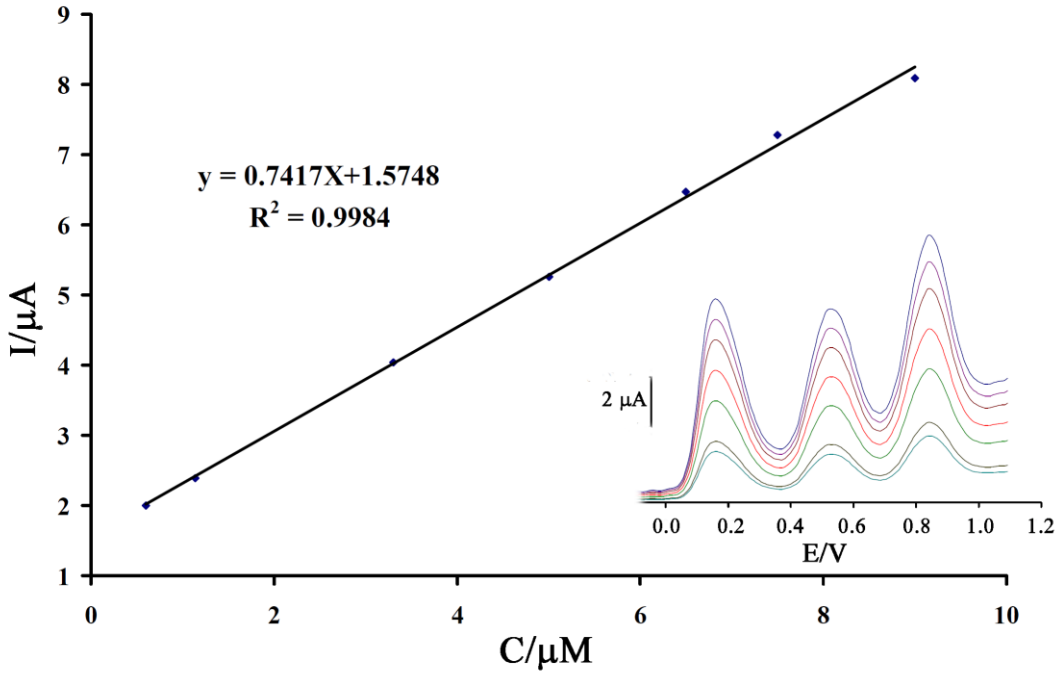

Figure 7. The plots of the electrocatalytic peak current as a function of HX concentration. Inset; SWVs of DMBQ/ZnO/CNTs/CPE in 0.1 MPBS (pH 8.0) containing different concentrations of HX–PL-ST in µM (from inner to outer): 0.6 + 36.5+ 20; 1.14 + 65.4+ 40.0; 3.3 + 126.0+109.3; 5.0 + 178.0+162.0; 6.5 + 247+ 216.5; 7.5+ 300+ 250 and 9.5+ 353+ 290 µM, respectively.

3.6. Stability and reproducibility

The reproducibility and stability of DMBQ/ZnO/CNTs/CPE was investigated by SWV measurements of 10.0 µM HX. The results showed that the relative standard deviation (RSD%) for five successive assays was 1.6%. In addition, the repeatability of the prepared modified electrode was checked using four different electrodes for the analysis of 10.0 µM HX, using SWV. The results showed a RSD% of 2.2%. Moreover, the stability of the modified electrode was examined by storing of the electrode in the lab at room temperature. Then, the electrode was used for the analysis of 10.0 µM HX using SWV. The results showed that the electrode signal retained to 97% of its initial response after two week and 93% of its initial response after 45 days. These results indicate that DMBQ/ZnO/CNTs/CPE has good stability and reproducibility, and could be used for HX measurements up to six week.

3.7. Interference study and real sample analysis

The influence of different substances as potential interfering compounds on the sensor selectivity were studied using 1.14 µM HX; 65.4µM PL and 40.0µM ST at pH 8.0. The tolerance limit

was taken as the maximum concentration of the foreign substances, which caused an approximately ±5% relative error in the determination. The results are shown in Table 1.

The applicability of the propose voltammetric sensor was checked with determination of HX, PL and ST in real samples such as tap water, river water, boiler water, wastewater, and well water. The determinations of HX, PL and ST in water samples were carried out using standard addition method (Table 2). The HX, PL and ST in water samples were also measured with published methods HX [2]; PL [46] and ST [5]. The results clearly demonstrate and confirm the capability of the modified electrode for the voltammetric determination of HX, PL and ST with high selectivity, accuracy, and good reproducibility.

Table 1. Interference study for the determination of 1.14 µM HX; 65.4 µM PL and 40.0 µM ST under the optimized conditions.

Species	Tolerance limits (W/W)
Glucose, Fructose, Lactose, Sucrose, Ethanol, Methanol	1000
Na^{+}, K^{+}, Cs^{+}, ClO_4^{-}, Ni^{2+}, CN^{-}, Ca^{2+}, Br^{-}, Ag^{+}, Zn^{+2}, Pb^{+2}, Mg^{2+}, Mn^{+2}, Co^{3+}, Cr^{2+}, and SCN^{-}	800
Urea	500

Table 2. Determination of HX, PL and ST in practical samples (n=3).

Sample	HX Added (µM)	PL Added (µM)	ST Added (µM)	Found (HX) Proposed method (µM)	Found (HX) Reference method (µM)	Found (PL) Proposed method (µM)	Found (PL) Published method (µM)	Found (ST) Proposed method (µM)	Found (ST) Published method (µM)
Tap water	-	-	-	< LOD	< LOD	< LOD	< LOD	< LOD	< LOD
	5.00	10.00	10.00	4.85 ± 0.45	5.44 ± 0.65	9.94 ± 0.35	10.65 ± 0.75	10.35 ± 0.55	10.84 ± 0.95
Well water	-	-	-	< LOD	< LOD	< LOD	< LOD	< LOD	< LOD
	15.00	20.00	20.00	15.35 ± 0.65	15.74 ± 0.95	20.24 ± 0.65	19.85 ± 0.72	20.75 ± 0.85	20.86 ± 0.87
River water [a]	-	-	-	< LOD	< LOD	< LOD	< LOD	< LOD	< LOD
	40.00	80.00	90.00	39.75 ± 0.82	40.74 ± 0.91	80.89 ± 1.01	80.65 ± 0.82	89.55 ± 1.15	90.32 ± 0.74
Waste water	-	-	-	< LOD	< LOD	< LOD	< LOD	< LOD	< LOD
	50.00	100.00	100.00	51.10 ± 1.22	50.96 ± 1.21	102.22 ± 2.27	101.65 ± 1.85	100.09 ± 1.10	102.85 ± 2.85
Boiler	-	-	-	< LOD	< LOD	14.98 ± 1.05	15.78 ± 0.85	5.54 ± 0.65	5.85 ± 0.65

[a] Tejan River, Sari, Iran

4. CONCLUSION

This work demonstrates the construction of a DMBQ/ZnO/CNTs/CPE and its application in the simultaneous determination of HX, PL and ST. The novel sensor showed excellent catalytic effects on the oxidation of HX. The results showed that the oxidation of HX is catalyzed at pH 8.0 and the peak potential of HX is shifted by 810 mV to a less positive potential at DMBQ/ZnO/CNTs/CPE. Potential differences of 370, 680 and 310 mV between HX–PL, HX–ST and PL–ST were detected respectively which were large enough to determine HX, PL and ST individually and/or simultaneously. Finally, this modified electrode used for determination of HX, PL and ST in the real samples such as water and wastewater.

ACKNOWLEDGEMENT
We are grateful to the Majlesi Branch, Islamic Azad University, Isfahan, Iran and the Iranian Nanotechnology Initiative Council for their support.

References

1. http://www.piercenet.com/product/hydroxylamine-hcl; 30, May, 2014.
2. R. Sadeghi, H. Karimi-Maleh, M.A. Khalilzadeh, H. Beitollahi, Z. Ranjbarha, M.B. Pasha Zanousi, *Environ. Sci. Pollut. Res*. 20 (2013) 6584–6593.
3. H. Karimi-Maleh, M. Moazampour, A.A. Ensafi, S. Mallakpour, M. Hatami, *Environ. Sci. Pollut. Res.* 21 (2014)5879–5888.
4. Agency for Toxic Substances and Disease Registry (ATSDR). Toxicological Profile for Phenol (Update). Public Health Service, U.S. Department of Health and Human Services, Atlanta, GA. 1998.
5. H. Karimi-Maleh, A.A. Ensafi, H. Beitollahi, V. Nasiri, M.A. Khalilzadeh, P. Biparva, *Ionics* 18 (2012) 687–694.
6. Tedmanson, Sophie (November 5, 2009). "Doctors risk untried drug to stop babys brain dissolving". The Times (London). Retrieved May 13, 2010.
7. H.R. Zare, N. Nasirizadeh, H. Ajamain, A. Sahragard, *Mat Sci Eng* C 31 (2011) 975–982.
8. H.R. Zare, Z. Sobhani, M. Mazloum-Ardakani, *Sens Actuators* B 126 (2007) 641–647.
9. H.R. Zare, F. Chatraei, N. Nasirizadeh, *J. Braz. Chem. Soc*. 21 (2010) 1977–1985.
10. A.A. Ensafi, H. Karimi-Maleh, M. Keyvanfard, *Intern. J. Environ. Anal. Chem*., 93 (2013) 650–660.
11. V. K. Gupta, A. K. Jain and G. Maheshwari, *Talanta* 72(4) (2007) 1469-1473.
12. V. K. Gupta, M. R. Ganjali, P. Norouzi, H. Khani, A. Nayak, and Shilpi Agarwal, *Critical Reviews in Analytical Chemistry,* 41(2011)282–313.
13. R. N. Goyal, V. K. Gupta, S. Chatterjee, *Sens. Actuators B. Chemical*, 149(2010) 252-258
14. V. K. Gupta, A. K. Jain, Shiva Agarwal, G. Maheshwari, *Talanta*, 71(2007)1964-1968
15. R. Jain, V. K. Gupta , N. Jadon, K. Radhapyari, *Analytical Biochemistry* 407 (2010) 79–88.
16. V.K. Gupta,A.K . Singh, S.Mehtab, B.Gupta, *Anal. Chim. Acta* 566 (2006) 5–10.
17. R.N. Goyal, V.K. Gupta, S. Chatterjee, *Electrochim. Acta* 53 (2008) 5354–5360.
18. V.K. Gupta, A.K. Singh,M. Al Khayat, Barkha Gupta, *Anal.Chim. Acta* 590 (2007) 81–90.
19. V.K. Gupta, R. Prasad, R. Mangla, P. Kumar,*Anal. Chim. Acta* 420 (2000) 19–27.
20. R.N. Goal, V.K. Gupta, S. Chatterjee, *Talanta* 76 (2008) 662–668.
21. A.A. Ensafi, H. Karimi-Maleh, S. Mallakpour, B. Rezaei, *Coll. Surf.* B 87 (2011) 480– 488

22. A.A. Ensafi, H. Karimi-Maleh, S. Mallakpour, M. Hatami, *Sens. Actuators* B 155 (2011) 464–472
23. H. Karimi-Maleh, P. Biparva, M. Hatami, *Biosens. Bioelect*. 48 (2013) 270–275.
24. J.B. Raoof, R. Ojani, H. Karimi-Maleh, *Electroanalysis* 20 (2008) 1259 – 1262
25. H. Bagheri, H. Karimi-Maleh, F. Karimi, S. Mallakpour, M. Keyvanfard, *J. Mol. Liq.* 198 (2014) 193–199.
26. H. Karimi-Maleh, F. Tahernejad-Javazmi, M. Daryanavard, H. Hadadzadeh, A.A. Ensafi, M. Abbasghorbani, *Electroanalysis* 26 (2014) 962-970.
27. H. Karimi-Maleh, M. Moazampour, H. Ahmar, H. Beitollahi, A.A. Ensafi, *Measurement* 51 (2014) 91–99.
28. H. Karimi-Maleh, A.L. Sanati, V.K. Gupta, M. Yoosefian, M. Asif, A. Bahari, *Sens. Actuators B* 204 (2014) 647–654.
29. A. Pahlavan, H. Karimi-Maleh, F. Karimi, M. Aboukazempour Amiri, Z. Khoshnama, M. Roodbari Shahmiri, M. Keyvanfard, *Mat. Sci. Eng. C* 45 (2014) 210-215.
30. T. Jamali, H. Karimi-Maleh, M.A. Khalilzadeh, *LWT - Food Science and Technology* 57 (2014) 679-685.
31. H. Karimi-Maleh, S. Mehdipour-Ataei, M. Hatami, M.A. Khalilzadeh, J. Anal. Chem, 69 (2014) 162-168.
32. M. Najafi, M.A. Khalilzadeh, H. Karimi-Maleh, *Food Chem.* 158 (2014) 125-131.
33. H. Beitollah, M. Goodarzian, M.A. Khalilzadeh, H. Karimi-Maleh, M. Hassanzadeh, M. Tajbakhsh, *J. Mol. Liq.* 173 (2012) 137-143.
34. T. Tavana, M.A. Khalilzadeh, H. Karimi-Maleh, A.A. Ensafi, H. Beitollahi, D. Zareyee, *J. Mol. Liq.* 168 (2012) 69–74.
35. M. Elyasi, M.A. Khalilzadeh, *Food Chem.* 141 (2013) 4311–4317.
36. A.J. Bard, L.R. Faulkner, *Electrochemical methods, fundamentals and applications,* Wiley, New York 2001.
37. Z. Galus, *Fundumentals of Electrochemical Analysis*, Ellis Horwood, New York 1976
38. A.A. Ensafi, H. Karimi-Maleh, *J. Electroanal. Chem*. 640 (2010) 75–83
39. H. Karimi-Maleh, M. Moazampoura,V.K. Gupta, A.L. Sanati, *Sens. Actuators* B 199 (2014) 47–53.
40. A.A. Ensafi, E. Khoddami, B. Rezaei, H. Karimi-Maleh, *Coll. Surf.* B 81 (2010) 42–49.
41. H. Karimi-Maleh, F. Tahernejad-Javazmi, A.A. Ensafi, R. Moradi, S. Mallakpour, H. Beitollahi, *Biosens. Bioelect*. 60 (2014) 1–7.
42. H. Karimi-Maleh, A.A. Ensafi, H.R. Ensafi, *J. Braz. Chem. Soc.* 20 (2009) 880-887.
43. H. Yaghoubian, H. Karimi-Maleh, M.A. Khalilzadeh, F. Karimi, *Int. J. Electrochem. Sci.,* 4 (2009) 993 – 1003.
44. M. Keyvanfard, M. Tahmasbi, H. Karimi-Maleh, K. Alizad, Chin. J. Catal. 35 (2014) 501–508.
45. R. Moradi, S.A. Sebt, H. Karimi-Maleh, R. Sadeghi, F. Karimi, A. Bahari, H. Arabi, *Phys. Chem. Chem. Phys.* 15 (2013) 5888—5897.
46. M. Wada, S. Kinoshita, Y. Itayama, N. Kuroda, K. Nakashima, *J. Chromatogr*. B 721 (1999)179–186.